Experimental Evaluation and Predictive Control of an Air-Cored Linear Generator for Direct-Drive Wave Energy Converters

Rieghard Vermaak, *Member, IEEE*, and Maarten J. Kamper, *Senior Member, IEEE*

***Abstract*—Direct-drive wave energy converters using linear generators (LGs) are attractive due to their high efficiency and reliability. Air-cored LGs, in particular, are receiving increasing attention due to the elimination of attraction forces between the stator and translator and the resulting reduction in structural mass. In this paper, details of the construction of a novel air-cored LG are presented. A custom test rig is constructed for testing the LG, particularly with zero overlap between its stator and translator at the stroke ends. Predictive control for maximum power transfer from the generator is first proposed and tested as a sensorless alternative to methods employing linear position feedback and electromotive force (EMF) estimation with sense coils. The control strategy is verified through simulation and measurements. It is also shown that allowing for zero stator–translator overlap at the stroke ends can improve the power-to-weight ratio compared to complete stator–translator overlap during the entire stroke.**

***Index Terms*—Air cored, direct drive (DD), linear generator (LG), predictive control, sensorless control, wave energy.**

NOMENCLATURE

$\mathbf{E_g}$	Generator EMF vector (V).
e_g	Instantaneous generator EMF (V).
e_r	Instantaneous rectifier voltage (V).
e_t	Instantaneous generator terminal voltage (V).
$\mathbf{I}$	Generator/rectifier current vector (A).
i	Instantaneous generator/rectifier current (A).
k_r	Current scaling factor.
L_s	Linear generator (LG) synchronous inductance (H).
L_f	Filter inductance (H).
P_g	Average generated power (W).
p_g	Instantaneous generated power (W).
p_t	Instantaneous power at generator terminals (W).
R_s	LG phase resistance (Ω).
T_s	Converter switching period (s).
$\mathbf{Z_g}$	Generator mechanical impedance vector (Ω).
$\mathbf{Z_s}$	Generator electrical phase impedance vector (Ω).

Manuscript received November 28, 2011; revised March 15, 2012; accepted April 23, 2012. Date of publication October 2, 2012; date of current version December 31, 2012. Paper 2011-EMC-608.R1, presented at the 2011 IEEE International Electric Machines and Drives Conference, Niagara Falls, ON, Canada, May 15–18, and approved for publication in the IEEE TRANSACTIONS ON INDUSTRY APPLICATIONS by the Electric Machines Committee of the IEEE Industry Applications Society. This work was supported by the South African National Energy Research Institute.

R. Vermaak is with the Distribution Division, Eskom Holdings SOC Ltd., Bellville 7530, South Africa (e-mail: rvermaak@ieee.org).

M. J. Kamper is with the Department of Electrical and Electronic Engineering, Stellenbosch University, Stellenbosch 7602, South Africa (e-mail: kamper@sun.ac.za).

Color versions of one or more of the figures in this paper are available online at http://ieeexplore.ieee.org.

Digital Object Identifier 10.1109/TIA.2012.2221671

I. INTRODUCTION

THE EARTH's oceans contain a massive amount of clean and sustainable energy in the form of its waves. Of all the different wave energy converters (WECs) that are currently being investigated, no superior technology is yet apparent though [1]; it is as such that commercial-scale wave energy is not yet a reality and that continued research in the field is necessary. Most WECs have some kind of primary mechanical interface which captures the wave energy. An intermediate power conversion stage, called the power takeoff (PTO), converts this captured energy to a form suitable for driving a conventional electrical generator. The PTO is usually a pneumatic or hydraulic system. Energy storage mechanisms in the form of hydraulic accumulators or flywheels are used for smoothing the variable energy captured from the waves. In many cases, a power converter at the generator output is also needed to further smooth out the power fed to the grid.

A technology which does stand out from the others in one aspect is direct drive (DD) WECs. In DD-WECs, the PTO is eliminated in order to reduce maintenance requirements and to increase reliability and efficiency; this makes it a very attractive option for the harsh environment of the ocean. With DD-WECs, the heave motion of the waves is used to directly drive an LG. A well-known example of such a device is the Archimedes Wave Swing (AWS) [2]. Some other DD-WECs in development can also be seen in [3]–[5]. The LG output varies in amplitude, frequency, and phase sequence due to the reciprocating motion of the WEC and the lack of inherent energy storage mechanisms. Some research focuses on LGs without application to a specific WEC, e.g., [6]–[9].

Due to this variation in the LG output, power electronic converters (PECs) with enough energy storage on the dc bus are essential for connecting the LG output to the grid. The aggregation of phase-shifted outputs of multiple LGs, however, relaxes the energy storage requirements as a natural smoothing effect occurs [10], [11]. Full-scale PECs will probably also be necessary in order to comply with the fault ride-through requirements of grid codes [12]. On the LG side, a PEC provides control of the LG current such that maximum power can be extracted from the WEC. Much research has addressed the issue of maximum power extraction from DD-WECs [13]–[18] and is also part of the focus of this paper.

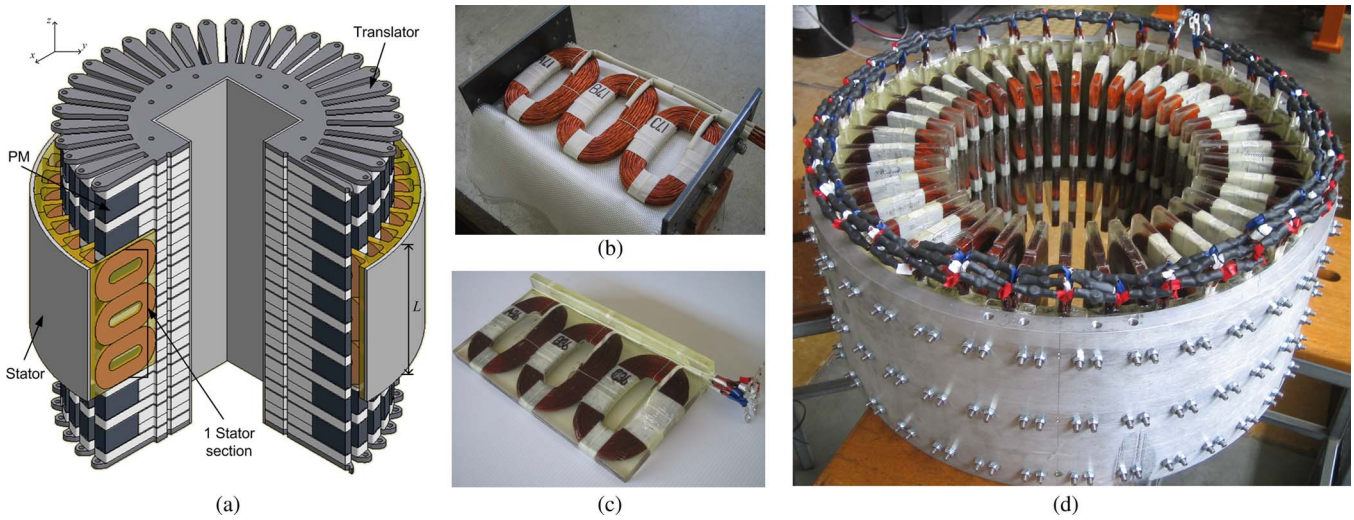

Fig. 1. (a) Three-dimensional cutout view of the novel air-cored PM LG. (b) Three preformed coils as laid up in the mold and (c) the finished stator section after removing from the mold. (d) Completed stator consisting of 38 molded stator sections bolted to the inside of an aluminum ring and connected in series.

Testing of LGs and their converters in the laboratory is not straightforward as linear drive systems are not commonplace in traditional electrical machine laboratories. Custom test rigs were, for instance, developed for laboratory testing of LGs in [4], [8], [14], [17], [19], and [20]. This includes vertical [4], [20] and horizontal [8] hydraulic drive systems, cable-and-pulley systems [14], [19], and a variable speed drive with a worm-and-ball gear [17]. Control hardware and software for such drive systems are also needed to simulate wave motion under a varying generator load. Developing a drive system for testing LGs can thus become a project on its own with considerable cost.

The authors of this paper developed a novel air-cored permanent magnet (PM) LG for use in DD-WECs which is discussed in Section II. A new laboratory test system is developed for the LG (see Section III) which allows testing of the proposed predictive control strategy (see Section IV) for the generator output. Simulation and test results are presented in Sections V and VI, respectively.

II. Experimental LG

A. Background

Because the heave motion of waves is rather slow (1–2 m/s peak) [17], the LGs in DD-WECs need to react very large forces in order to generate a significant amount of power. The LGs therefore become very large and expensive. The LGs of the AWS [2], Uppsala University [3], and Oregon State University [4] are among the only ones which have been tested in the sea; all of these are iron-cored longitudinal-flux LGs. Because the LGs are so large, the attractive forces between the PM translator and iron-cored stators are also very large and pose significant challenges in terms of bearing design and construction of the machine. Structural material for supporting these attractive forces also contributes significantly to the WEC's overall cost. Cogging forces, particularly due to pairwise flux coupling and the longitudinal ends of iron-cored generators, also cause problems [4], [21].

Due to the previously named issues, air-cored and slotless LGs are receiving increasing attention for use in DD-WECs [5], [7]–[9], [17], [18], [20]. Despite using more PM material than a comparable iron-cored machine, the elimination of cogging forces and the elimination of the attraction forces between the stator and translator make air-cored generators worth the while in this case. Trident Energy uses a tubular slotless (air cored with an iron yoke) LG in its WEC [5], [20]. A similar entirely air-cored LG is investigated in [7] and [17]. At Edinburgh University, a novel linear double-sided (LDS) PM translator air-cored topology named the C-Gen is currently being developed [8]. By using an LDS PM translator, a higher air gap flux density than that in a single-sided air-cored machine can be maintained. However, attractive forces between the two opposing translator sides are now introduced which again creates the need for increased structural mass.

B. The Novel Air-Cored PM LG

The authors developed a novel air-cored topology from the LDS machine, and this is shown in Fig. 1(a). The topology evolved by placing a number of LDS machines in a tubular topology, removing the iron yokes and merging adjacent magnets. The flux from any magnet now circulates transversely around the machine while each magnet experiences an ideally equal force from either side (i.e., the net force is ideally zero). The effect is that very little structural material is needed for PM support. The stator consists of a number of separate sections which are inserted between the PMs. The design and optimization of a 1-kW prototype of the novel LG is reported in [9]. More details on the construction and test setup are given in [18] and are expanded on in this paper.

Each separate stator section consists of nonoverlapping concentrated coils cast into epoxy resin for support. Sixteen strands of 0.5-mm copper wire were twisted together to form a litz wire; this limits the eddy-current losses in the copper wire. The litz wire was then wound around a former to create the preformed coils, as shown laid up in a mold in Fig. 1(b). Epoxy

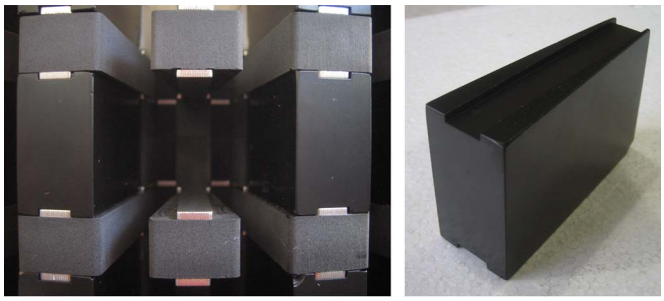

(a) (b)

Fig. 2. (a) Close-up of the translator with one PM removed; the layers of (dull black) plastic and stainless steel are evident. (b) One PM showing the tapered shape and the grooves at the top and bottom into which the stainless steel strips slide.

resin was cast around three of the preformed coils (for three phases) to form a finished stator section, as shown in Fig. 1(c). The completed stator, as seen in Fig. 1(d), consists of 38 of these sections bolted to the inside of an aluminum ring. The winding and casting was by far the most labor- and time-intensive process in the construction of the machine.

The translator was constructed from layers of engineering plastic and thinner layers of nonmagnetic stainless steel pressed over a square steel pipe. These layers can be seen in the computer-aided design model in Fig. 1(a) and are also shown close-up in Fig. 2(a). The plastic forms the nonmagnetic spacers between the magnets, and the stainless steel serves as a more rigid nonmagnetic support for the PMs. The PMs, as shown in Fig. 2(b), are slightly tapered and have grooves at the top and bottom for the stainless steel to slide into; they were therefore simply slid into place from the outside. Assembling the translator was easy and fast compared to the stator construction.

C. Electrical Properties

The per unit phase resistance and synchronous reactance are 0.17 p.u. and 0.026 p.u., respectively. The designed pole width of 56 mm and nominal translator velocity of 0.75 m/s result in an electrical frequency of 6.7 Hz. As mentioned before, the low operating speed requires a relatively large amount of active material for a given power output. This fact is evident in the novel LG as the phase resistance is rather high. The synchronous reactance is, in turn, rather low and also very linear due to the lack of iron in the stator core and the low electrical frequency. A low load angle of 8.7° at nominal load results from this. This is an important advantage for LGs used in DD-WECs. In [3], it is shown how an inherently low load angle at nominal power results in better voltage regulation at overload conditions (which are frequently experienced in the sea). It, of course, also eliminates the need for phase compensation equipment such as capacitors. In [13], for instance, a very much overrated active rectifier is used for phase compensation of an LG with a high load angle.

D. Translator Length

For LGs, the PM translator is usually made to be longer than the stator such that the whole stator winding is active during as much of the stroke length as possible. If the whole stator winding is to be active during the *entire* stroke, the translator length must be

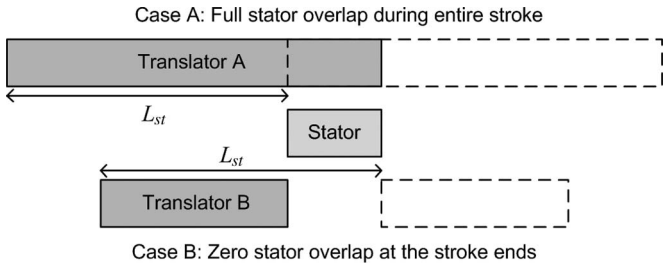

Fig. 3. Translator length for a given stator and stroke length: Case A represents full stator–translator overlap during the entire stroke, whereas Case B represents zero stator–translator overlap at the stroke ends.

$$L_{tA} = L_{st} + L \tag{1}$$

where L_{st} is the stroke length and L is the stator length. This situation is illustrated by Case A in Fig. 3; the resultant PM translator can be very long and expensive.

An alternative approach followed for the air-cored LGs in [8] and [17] is to purposefully make the translator shorter than the stator in order to save on PM cost. Measures are, however, needed to switch the inactive coils out of the circuit such that they do not contribute to conduction losses. In [8], a displacement transducer is used to determine when to switch each stator coil in or out with a triac. In [17], all the stator coils are paralleled onto a common dc bus through individual boost converters; the converters effectively isolate inactive coils from the dc bus. The large number of power electronic components needed for these schemes is, however, a drawback.

For the novel LG, it was theorized that the power-to-weight ratio could be improved by shortening the translator of Case A in Fig. 3 such that the whole stator becomes inactive at the stroke ends as shown for Case B in Fig. 3. At the stroke ends, the velocity, and generated power, is at its lowest, and the conduction losses incurred by allowing the coils to become inactive will also be very low; hence, no effort is made to switch the inactive coils out of the circuit as in [8] and [17]. For Case B and with the same stroke and stator length as in Case A, the translator length now becomes

$$L_{tB} = L_{st} - L. \tag{2}$$

From (1) and (2), it is clear that, for a fixed stroke and stator length, the translator length can be significantly shorter, and cheaper, in Case B than in Case A.

To investigate the effect on the power output of the novel LG, finite element (FE) simulations of one stroke of Cases A and B are conducted (the finite element analysis (FEA) modeling is discussed in [9]). In Fig. 4(a) and (b), the electromotive force (EMF) waveforms of Cases A and B are respectively shown. Assuming that the LG current is proportional to the EMF as

$$i(t) = k_r e_g(t) \tag{3}$$

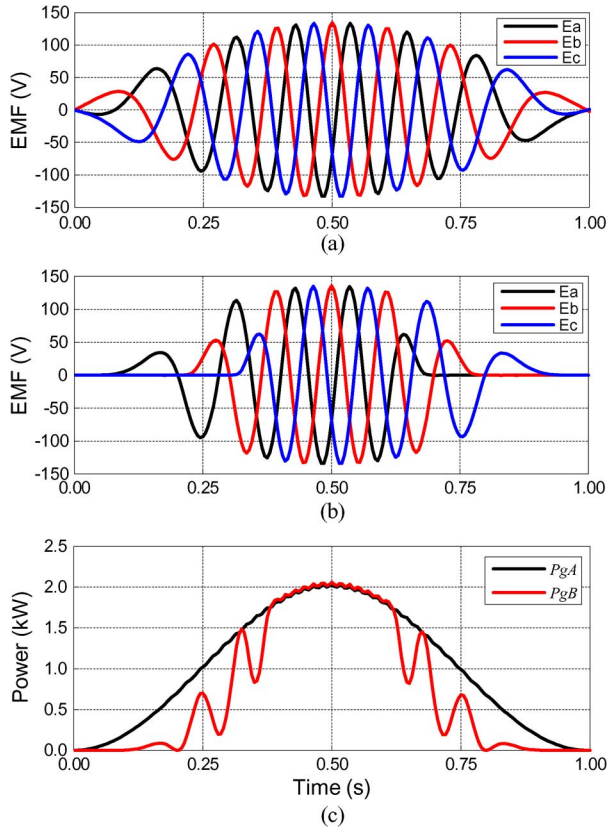

Fig. 4. FE-simulated LG EMFs over one stroke length for (a) Case A and (b) Case B. (c) LG instantaneous generated power for Cases A and B.

TABLE I
COMPARISON OF THE POWER PER PM MASS BETWEEN CASES A AND B

Parameter	Case A	Case B
Stator length (m)	0.224	0.224
Stroke length (m)	0.672	0.672
Translator length (m)	0.896	0.448
Average generated power (W)	1005	734
Power per PM mass (p.u.)	1	1.46

where k_r is the current scaling factor, the instantaneous generated power is calculated from the FE-obtained EMF waveforms as

$$\begin{aligned} p_g(t) &= e_{ga}(t)i_a(t) + e_{gb}(t)i_b(t) + e_{gc}(t)i_c(t) \\ &= k_r\left[e_{ga}^2(t) + e_{gb}^2(t) + e_{gc}^2(t)\right]. \end{aligned} \tag{4}$$

A value of $k_r = 0.074$ gives the rated power as designed in [9].

The instantaneous generated power for Cases A (p_{gA}) and B (p_{gB}) is shown in Fig. 4(c). The average power generated in Case A is 1005 W, while in Case B, it is 734 W. The stator, translator and stroke length, and average generated power for both cases are also given in Table I. If the per unit power per PM mass in Case A is taken as unity, the power per PM mass in Case B turns out to be 1.46 p.u. Although the stroke and translator length of this LG was not designed for a real sea state, this result shows that, from a cost perspective, it could make sense to allow for zero overlap between the stator and translator at the stroke ends.

The loss of translator control at the stroke ends will need to be taken into account though. Careful consideration should be given to whether this situation is allowable for an actual DD-WEC installation. Furthermore, a large degree of phase unbalance is observed near the stroke ends in Fig. 4(b), which causes large dips in power as shown in Fig. 4(c). This is, of course, highly undesirable and is made worse by the particular prototype stator winding layout, which has only one concentrated coil per phase along the whole length of the stator, as shown in Fig. 1(a). However, for a larger LG, it is expected that more coils per phase will be distributed along the length of the stator which will considerably reduce the dips in power observed in Fig. 4(c).

III. TEST SETUP

The completed prototype LG and the laboratory drive system are shown in Fig. 5, and a schematic diagram of the entire test setup for the LG is shown in Fig. 6. Since a relatively simple and cheap solution for a test rig was sought, use was made of existing equipment as far as possible. This entailed modifying and reusing an existing experimental 20-kW 40-pole PM wind turbine generator (WTG) and back-to-back two-level insulated-gate bipolar transistor (IGBT) voltage source converters (VSCs) which were used for the grid connection of the WTG. The VSCs included a Texas Instruments TMS320F28335 32-b floating-point digital signal controller (DSC) for implementing control calculations.

The WTG was fitted with a crankshaft for converting its rotation to translation for driving the LG. The LG was mounted horizontally with its stator suspended on linear tracks (as shown in Fig. 5). Since the stator is much lighter than the translator, it is easier to move the stator rather than the translator. The WTG was mounted with its axis vertical, and its back plate was replaced with a slightly larger one to provide the required stroke length. One VSC is used to drive the WTG as a motor, and another one is used as an active rectifier for the LG output. The energy in the system is effectively circulated through the motor, the LG, and the dc bus. The dc bus is manually charged up from the grid through a variac and a diode rectifier; the losses in the system are supplied from the grid to the dc bus.

By using the arrangement in Fig. 6, a regulated dc bus is assumed. Also, no provision is made for the grid connection of the LG output. In a real wave power plant, the power from a number of DD-WECs will probably feed onto a common dc bus from where it will then be inverted to the grid [10], [11], [22]. Attempting dc-bus voltage regulation and grid connection of only one LG is therefore deemed as an unnecessary exercise.

A filter is installed between the active rectifier and the LG. The main reason for this is that the LG's terminal voltage must be measured in the control strategy described in Section IV-B, and hence, the high switching frequency must be filtered out. There are, however, also a number of other reasons why the use of a filter is justified. Pulsewidth modulation (PWM) voltages applied to machines have been shown to cause a number of undesirable effects, as, for instance, discussed in [23]–[25]; this includes excessive winding insulation stress due to high dv/dt and voltage reflections when the cable between the machine

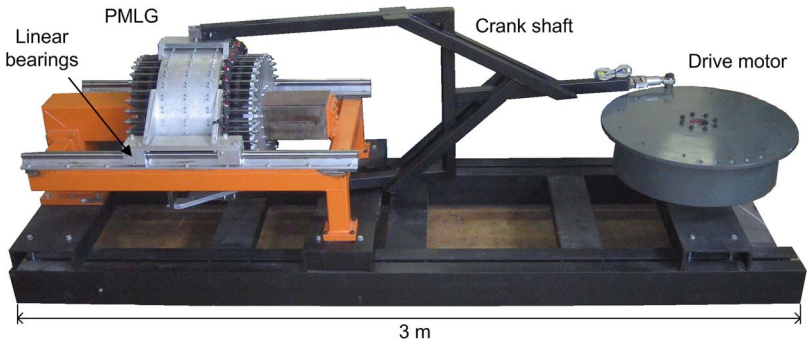

Fig. 5. Prototype LG and drive motor in the laboratory test setup.

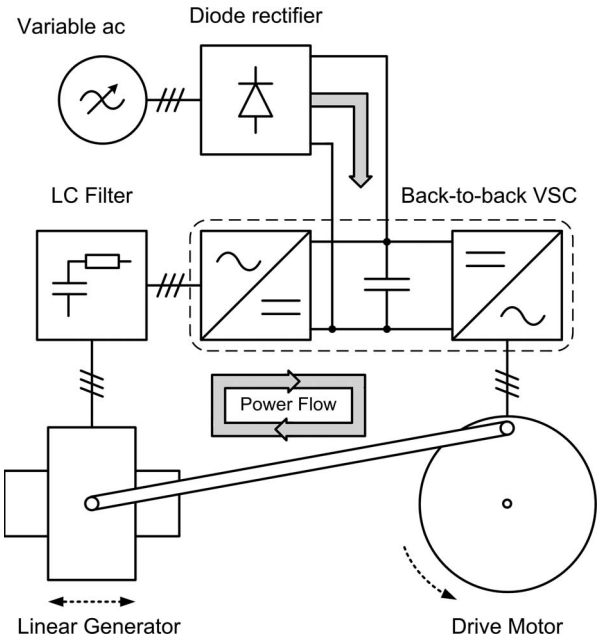

Fig. 6. Schematic diagram of the unique LG test setup.

and drive is long. Radiated and conducted electromagnetic interference, which can respectively cause malfunction of electronic devices and additional system losses, are also problematic. These unwanted effects can be reduced, if not eliminated, with a filter. A simple LC filter is a robust and cost-effective solution [24] and is hence used here. Since the LG operates at very low frequencies, the voltage drop across the filter is expected to be almost negligible.

IV. Power Conversion Control

A. Background

The theory on energy absorption from the waves is covered in [1], [15], and [26]. The energy conversion process in DD-WECs can be seen in terms of the mechanical energy absorbed from the waves by the front-end mechanical interface (e.g., the buoy) and the electrical energy absorbed from the LG by the load. In simplified terms, these energy conversion steps can be modeled with lumped parameter electrical circuits as shown in Fig. 7.

The internal wave impedance $\mathbf{Z_w}$ represents the hydrostatic buoyancy, the friction, and the wave radiated by the device [26]. From classical circuit theory, it is known that maximum

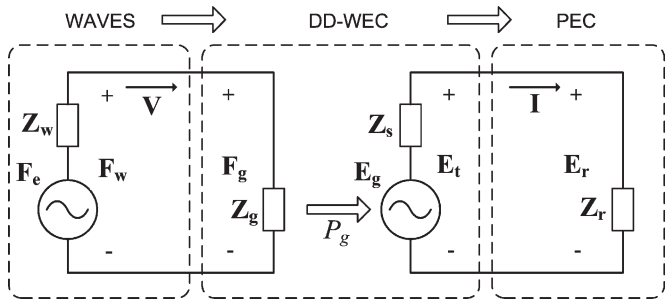

Fig. 7. Simplified lumped parameter electrical circuit modeling of the energy conversion process from the waves to the DD-WEC and to the PEC.

energy is transferred to the load $\mathbf{Z_g}$ (the WEC) when the device velocity $\mathbf{V}$ is in phase with the wave excitation force $\mathbf{F_e}$ and with

$$\mathbf{Z_g} = \mathbf{Z_w^*}. \tag{5}$$

This effectively constitutes a resonance condition between the waves and the WEC. This condition can be achieved by controlling the WEC's reaction to the waves with mechanical means; the AWS is such an example, where the imaginary part of $\mathbf{Z_g}$ is directly controlled by adjusting the air pressure and water volume in the device [2]. The condition can also be achieved purely electrically by manipulating the LG current, and hence $\mathbf{F_g}$ from Fig. 7, with the PEC [15], [16], [19].

Device reaction force control with a PEC has obvious advantages over mechanical actuators like in the AWS, e.g., faster operation, lower maintenance, and greater flexibility. However, reaction force control will always cause a phase difference between the LG current $\mathbf{I}$ and EMF $\mathbf{E_g}$ as reactive power needs to be returned to the waves during part of the period; the condition for maximum power transfer between the LG and load is therefore compromised.

As the prototype novel LG is not device specific, optimal mechanical energy capture is ignored here, and the focus is only on controlling power transfer between the LG and load, as is also done in [13] and [17].

B. Proposed Control Strategy

Assuming that the translator velocity and developed force are both sinusoidal and in phase, the LG current should be controlled to be proportional to the EMF as already given in (3). The EMF can, however, not readily be measured while on load. Sense coils mounted on the stator [5], [13], [15], [19] or

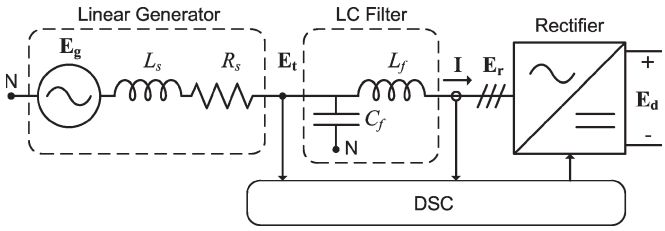

Fig. 8. Single line diagram of the LG, filter, and active rectifier.

wrapped around the stator windings [17] are, in some cases, used to estimate the EMF amplitude and phase for control purposes. The authors of [13], however, admit that this is a cumbersome practice and that sensorless control methods should instead be investigated.

In this paper, a deadbeat control strategy, as discussed in [27] and [28], is proposed for the LG current control. Deadbeat control is a type of predictive control [29]; the principle of this inherently digital type of control is to calculate the PEC voltage necessary to force the measured current to its reference value by the following modulation period [27], [29]. The calculation of the PEC voltage reference must be based on an accurate system model and accurate knowledge of the system parameters such as resistance and inductance [27].

Similar to predictive control, the system model is also used to calculate the stator flux linkage in one type of position-sensorless control [30]. Instead of using a position sensor, the calculated stator flux linkage is then used to derive position information which can be used in the chosen control strategy. Predictive control can therefore be seen as one way of achieving sensorless control, as, for instance, in [31]. In this paper, a similar approach is also used to calculate the EMF without the use of position feedback or estimation; this is further discussed in the next section.

Space vector PWM (SV-PWM), which is ideally suited to digital control, is used to generate the IGBT gating signals as discussed in [32]. For this, the measured current and voltages should first be transformed to the stationary two-coordinate $\alpha\beta$-reference frame. It is often preferred to transform measured quantities to the synchronously rotating dq-reference frame where all electrical quantities are constant at steady state [33]. For the constantly changing translator velocity of an LG, there is, however, no steady state, and hence, even in the dq-reference frame, electrical quantities are constantly changing, as, for instance, shown in [16]. In addition, translator position feedback or estimation and decoupling transformations are needed in order to do control calculations in the dq-reference frame. In order to avoid especially the translator position feedback or estimation, control calculations are here done in the $\alpha\beta$-reference frame. The same approach is followed for predictive control in [27], [34], and [35]. In [35], control calculations are done in both the $\alpha\beta$- and dq-reference frames, and similar results are demonstrated in both cases.

C. Predictive Control Calculations

A single line diagram of the LG connected to the PEC through the LC filter is shown in Fig. 8. It is assumed that only the switching frequency currents flow through the filter capacitor C_f; these currents are ignored, and it is as such assumed that the measured rectifier current $\mathbf{I}$ is the same as the LG current. In terms of the measured instantaneous LG terminal voltage $e_t(t)$ and instantaneous rectifier current $i(t)$, the rectifier voltage $e_r(t)$ is given as

$$e_r(t) = e_t(t) - L_f \frac{di(t)}{dt} \tag{6}$$

where L_f is the filter inductance. Writing this as a difference equation for digital implementation gives

$$e_r[k] = e_t[k] - \frac{L_f}{T_s}\left(i[k+1] - i[k]\right) \tag{7}$$

where T_s is the switching period. If the current error is given as $\varepsilon_i[k] = i^*[k] - i[k]$, the deadbeat condition gives $\varepsilon_i[k+1] = 0$ [28]. This means that $i[k+1]$ must equal the reference current $i^*[k]$. Substituting this into (7) then gives the rectifier voltage needed to achieve the deadbeat condition as

$$e_r^*[k] = e_t[k] - \frac{L_f}{T_s}\left(i^*[k] - i[k]\right). \tag{8}$$

D. EMF Calculation

From Fig. 8, the LG model is given by

$$\begin{aligned} e_t &= \frac{d\lambda(t)}{dt} - i(t)R_s \\ &= e_g(t) - L_s\frac{di(t)}{dt} - i(t)R_s \end{aligned} \tag{9}$$

where λ is the total stator flux linkage. As mentioned before, position information can be derived from the stator flux linkage which can be found by rearranging and integrating (9) as

$$\lambda(t) = \int \left[e_t(t) + i(t)R_s\right] dt. \tag{10}$$

In this application, only the instantaneous EMF is required for the current reference calculation from (3) and not the position. This greatly simplifies the required calculation. Furthermore, since the synchronous inductance of the novel LG is negligible compared to the phase resistance (from Section II-C), the LG's EMF can then simply be calculated from (9) as

$$e_g[k] = e_t[k] + i[k]R_s. \tag{11}$$

By substituting (11) into (3), the reference current in (8) can now be calculated as

$$i^*[k] = k_r(e_t[k] + i[k]R_s). \tag{12}$$

The control strategy is shown schematically in Fig. 9.

V. Simulation

The LG, filter, and active rectifier as shown in Fig. 8 were implemented in the multidomain simulation package Ansys Simplorer for verification. The data from the FE-simulated EMFs shown in Fig. 4(b) are stored in a lookup table and used as reference for ideal voltage sources representing the LG's EMFs. The rectifier is modeled with ideal switches representing the IGBTs, and an ideal dc voltage source is used to represent

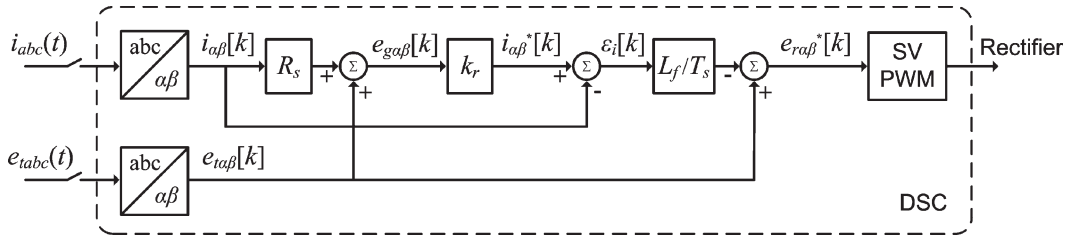

Fig. 9. Predictive control calculation and SV-PWM as implemented in the DSC.

TABLE II
PROTOTYPE LG AND PEC PARAMETERS

Phase resistance R_s (p.u.)	0.17
Synchronous reactance X_s (p.u.)	0.026
Filter inductance L_f (mH)	1.3
Filter capacitance C_f (μF)	23.5
Switching frequency f_s (kHz)	20
DC bus voltage E_d (V)	300

the dc bus. The parameters as used in the simulation are given in Table II. Simplorer includes a VHDL-AMS solver, and therefore, the control and SV-PWM calculations were implemented with VHDL code as described in [36].

In Fig. 10(a), the simulated currents injected to the converter during one stroke under predictive control are shown. The current amplitudes deviate from the ideal sinusoidal envelope at the stroke ends; this can be expected when considering the EMFs of Fig. 4(b). In Fig. 10(b), the c-phase EMF, terminal voltage, and current are shown. During the first part of the stroke, the a-phase and b-phase become active first. It can be seen that, since the three phase currents are balanced, current from the a- and b-phases is conducted through the c-phase before it becomes active itself, i.e., while the c-phase EMF is still zero. This transitional phase current can be seen to be 180° out of phase with the terminal voltage during this time and therefore only constitutes losses. As the c-phase becomes active, the current and terminal voltage can be seen to track the EMF. The current is in phase with the EMF as required. The terminal voltage is also in phase with the EMF and highlights the small effect of the synchronous inductance.

The c-phase current (i_c) is shown in Fig. 10(c) together with the ideal reference current (i_{cr}), as scaled from the known EMF according to (3), and the reference current (i_{crc}) calculated in the control algorithm from (8)–(10). The transitional phase currents from the a- and b-phases during the start of the stroke cause the calculated reference to deviate from the ideal reference. The simulated current follows the calculated reference current almost exactly.

The ideal instantaneous three phase generated power (p_{gi}), as calculated from (4) and also shown in Fig. 4(c), the simulated generated power (p_g), and the power transferred (p_t) from the LG are shown in Fig. 10(d). The simulated power p_g deviates slightly from the ideal waveform of p_{gi} at the stroke ends due to the additional losses incurred by the transitional phase currents. The average value of p_g is $P_g = 700$ W, almost 5% less than P_{gi}. The power at the LG terminals, which is transferred to the filter–PEC combination, is calculated as $P_t = 602$ W; this results in an LG efficiency of $\eta = P_t/P_g = 86\%$ (ignoring eddy-current losses).

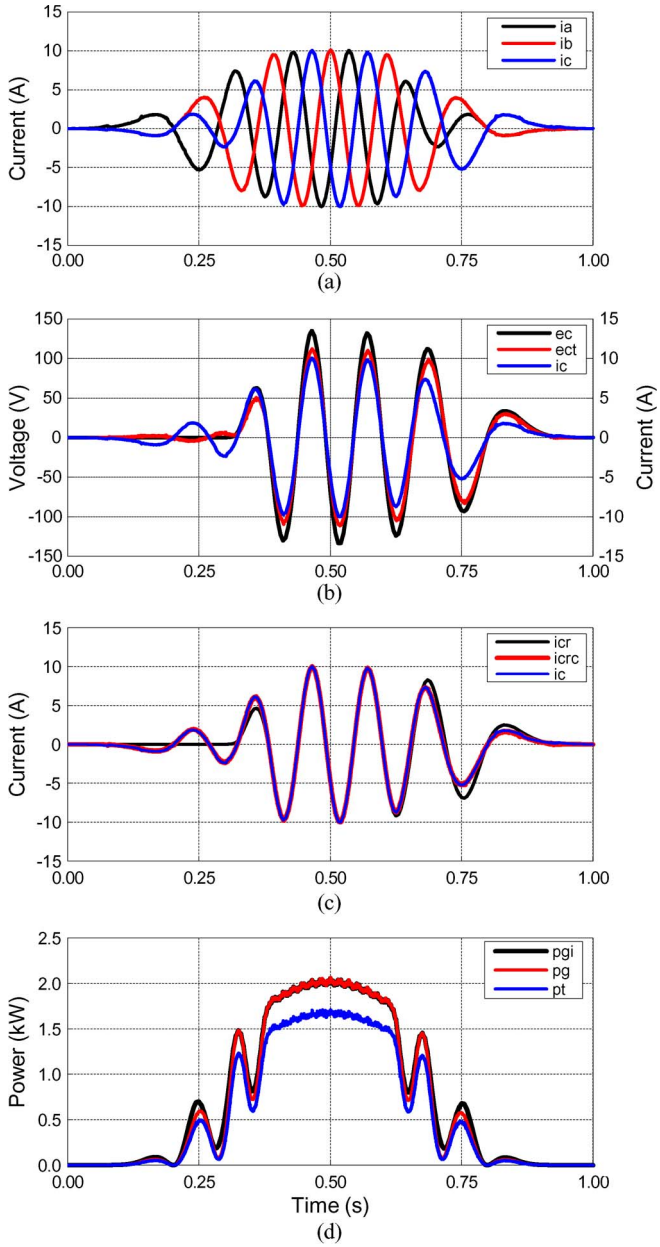

Fig. 10. Simulation of the predictive control yields (a) the three phase currents injected to the converter; (b) c-phase EMF (e_c), terminal voltage (e_{tc}), and current (i_c); (c) c-phase ideal reference current (i_{cr}), reference current as calculated in the control (i_{crc}), and the simulated current (i_c); and (d) the ideal three phase instantaneous generated power (p_{gi}), the simulated instantaneous generated power (p_g), and the instantaneous power injected to the rectifier (p_t).

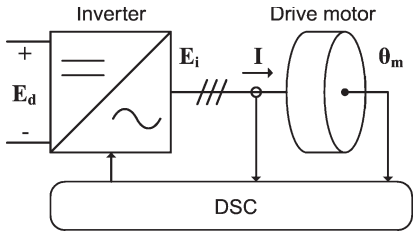

Fig. 11. Single-line diagram of the drive motor and inverter.

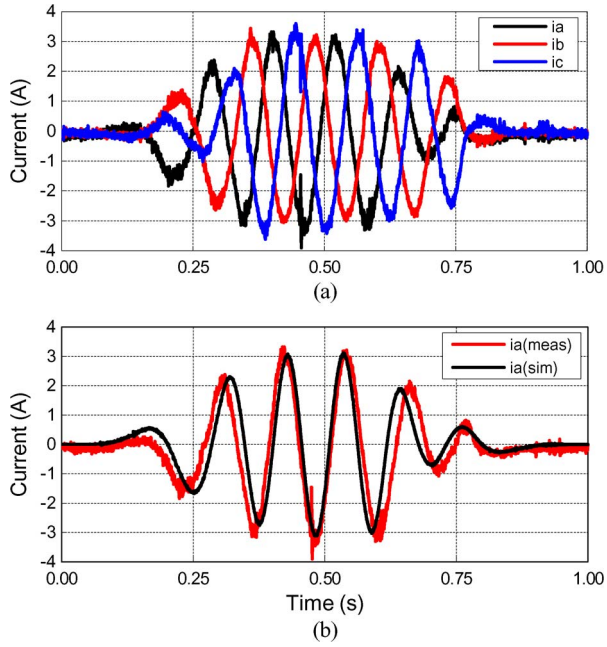

Fig. 12. Measurements with $k = 0.023$ showing (a) the three phase currents as injected to the rectifier and (b) the measured and simulated a-phase currents.

VI. Test Results

The SV-PWM and control calculations from (8)–(10) are implemented with the DSC. Apart from the LG control, a normal field-oriented control algorithm for controlling the drive motor speed is also implemented. The drive motor is fitted with a resolver which enables position feedback necessary for the dq-transformation of the motor currents as shown in Fig. 11. The outer speed control loop provides a q-axis current reference to the inner current control loop; the d-axis current reference is kept equal to zero. Controlling the drive motor speed at a constant value while the LG is on load is necessary to reproduce the sinusoidal displacement profile of the translator as simulated.

In [9], the LG's terminal voltages under no-load conditions are shown to correspond very well with the FE-simulated EMF waveforms of Fig. 4(b); this serves to validate the FE modeling and design and also verifies that the drive motor speed control works correctly. Further tests done in [9] show that the LG current and terminal voltage are basically in phase with simply a resistive load connected. This confirms the small effect of the synchronous inductance.

Some mechanical problems were, however, experienced with the drive system, and testing was only possible at up to about 30% of full load. A current scaling factor of $k_r = 0.023$ in the predictive control was used to produce the measured three phase currents shown in Fig. 12(a) with the LG connected to the rectifier. The wave shapes clearly correspond very well with the simulated currents shown in Fig. 10(a). The simulation is repeated with the reduced scaling factor, and in Fig. 12(b), the measured a-phase current is shown together with the simulated current for the same conditions. Very good agreement between the two is observed. The phase shift between the measured and the simulated waveform at times is due to the fact that the drive motor speed cannot be controlled to be exactly constant during the stroke.

VII. Discussion

Even though rated conditions could not be tested, the test results show that the predictive control works as expected. The fact that the LG's phase resistance can be measured fairly accurately and that the synchronous inductance is negligibly small clearly aids in the easy and accurate calculation of the LG's EMFs (and hence the reference currents). For iron-cored LGs, the effect of the inductance in (9), which is generally much higher than that in air-cored machines, will have to be taken into account. Translator position estimation may also be necessary, depending on the degree of position dependence of the inductance, which, in turn, very much depends on the PM translator structure [30]. In this case, the straightforward control calculations as presented in Section IV-D will become more complex. Furthermore, parameter sensitivity is a well-documented issue in predictive control. This issue is not addressed here and will have to be investigated in more detail in the future. Methods have been proposed to make deadbeat control more robust against parameter mismatch [27], [28], [34], and some of these methods could be incorporated here.

The prototype LG was designed for nominal velocity, and the test setup was designed to verify the LG operation specifically at nominal velocity. A real DD-WEC will, however, be subjected to a large variation in both stroke length and velocity, and future work should focus on evaluating the LG for these varying conditions. This also includes the working of the control strategy.

It is shown that the cost of the LG can possibly be significantly reduced by decreasing the amount of overlap between the stator and translator at the stroke ends. This, however, also results in a small reduction in generated power. In this paper, the total effect was evaluated in terms of the generated power per PM mass. The nonideal operation of the control during the period of phase unbalance at the stroke ends causes a further reduction in generated power. In order to determine whether these effects are acceptable, a complete evaluation of capital cost versus income needs to be done. At this stage of the prototype testing, this is, however, not possible, as actual sea conditions, total system losses, and material and electricity prices need to be considered. All of these aspects are location specific and constantly changing. Such an economic evaluation would therefore, at this stage, not yet be meaningful.

VIII. Conclusion

It is shown through FEA that allowing for zero overlap between the stator and translator at the stroke ends of LGs can improve the power-to-weight ratio compared to LGs designed for full stator–translator overlap during the entire stroke. In this

particular case, a 46% increase was found, although it must be mentioned that the stroke length of the LG of this paper was not designed for actual wave heights. For a real installation, the actual wave conditions must be taken into account, and consideration must be given to whether the sacrifice in control at the stroke ends with zero stator–translator overlap will be allowable.

A deadbeat predictive control method, as an alternative to previously proposed LG control strategies, is here shown to work well in terms of forcing the current to follow the calculated reference very closely without the need for linear position or EMF sensing. During the transitional phase, where the stator–translator overlap is changing, the calculated reference, however, deviates slightly from the ideal reference, which is scaled from the actual EMF. Control stability is maintained, but it results in a 5% loss in power from the ideal generated power. Take note, however, that this loss is incurred after the aforementioned increase in the power-to-weight ratio gained by allowing for zero stator–translator overlap at the stroke ends.

The low inductance of the air-cored stator winding and the fact that position information is not needed are shown to greatly simplify the control calculation. For typical iron-cored LGs, the strategy will have to be adapted to include the effect of the higher nonlinear inductance and will hence increase the complexity of the control problem.

ACKNOWLEDGMENT

Opinions expressed and conclusions arrived at are those of the author and are not necessarily to be attributed to the South African National Energy Research Institute.

REFERENCES

[1] A. F. D. O. Falcão, "Wave energy utilisation: A review of the technologies," *Renew. Sustain. Energy Rev.*, vol. 14, no. 3, pp. 899–918, Apr. 2010.

[2] H. Polinder, M. E. C. Damen, and F. Gardner, "Linear PM generator system for wave energy conversion in the AWS," *IEEE Trans. Energy Convers.*, vol. 19, no. 3, pp. 583–589, Sep. 2004.

[3] O. Danielsson, M. Eriksson, and M. Leijon, "Study of a longitudinal flux permanent magnet linear generator for wave energy converters," *Int. J. Energy Res.*, vol. 30, no. 14, pp. 1130–1145, Nov. 2006.

[4] J. Prudell, M. Stoddard, E. Amon, T. K. A. Brekken, and A. von Jouanne, "A permanent-magnet tubular linear generator for ocean wave energy conversion," *IEEE Trans. Ind. Appl.*, vol. 46, no. 6, pp. 2392–2400, Nov. 2010.

[5] P. C. J. Clifton, R. A. McMahon, and H. P. Kelly, "Design and commissioning of a 30 kW direct drive wave generator," in *Proc. IET 5th Int Conf. Power Electron., Mach. Drives*, Brighton, U.K., 2010, pp. 1–6.

[6] M. A. Mueller and N. J. Baker, "Modelling the performance of a vernier hybrid machine," *Proc. Inst. Elect. Eng.—Elect. Power Appl.*, vol. 150, no. 6, pp. 647–654, Nov. 2003.

[7] M. A. Mueller, N. J. Baker, L. Ran, N. G. Chong, H. Wei, P. J. Tavner, and P. McKeever, "Experimental tests of an air-cored PM tubular generator for direct drive wave energy converters," in *Proc. IET 4th Int. Conf. Power Electron., Mach. Drives*, York, U.K., 2008, pp. 747–751.

[8] N. Hodgins, O. Keysan, A. S. McDonald, and M. A. Mueller, "Design and testing of a linear generator for wave energy applications," *IEEE Trans. Ind. Electron.*, vol. 59, no. 5, pp. 2094–2103, May 2012.

[9] R. Vermaak and M. J. Kamper, "Design aspects of a novel topology air-cored permanent magnet linear generator for direct drive wave energy converters," *IEEE Trans. Ind. Electron.*, vol. 59, no. 5, pp. 2104–2115, May 2012.

[10] B. Das and D. C. Pal, "Voltage control performance of AWS connected for grid operation," *IEEE Trans. Energy Convers.*, vol. 21, no. 2, pp. 353–361, Jun. 2006.

[11] K. Thorburn and M. Leijon, "Farm size comparison with analytical model of linear generator wave energy converters," *Ocean Eng.*, vol. 34, no. 5/6, pp. 908–916, Apr. 2007.

[12] D. L. O'Sullivan, G. Dalton, and A. W. Lewis, "Regulatory, technical and financial challenges in the grid connection of wave energy devices," *IET Renew. Power Gener.*, vol. 4, no. 6, pp. 555–567, Nov. 2010.

[13] P. R. M. Brooking and M. A. Mueller, "Power conditioning of the output from a linear vernier hybrid permanent magnet linear generator for use in direct drive wave energy converters," *Proc. Inst. Elect. Eng.—Gener. Transm. Distrib.*, vol. 152, no. 5, pp. 673–681, Sep. 2005.

[14] V. D. Colli, P. Cancelliere, F. Marignetti, and R. Di Stefano, "A tubular-generator drive for wave energy conversion," *IEEE Trans. Ind. Electron.*, vol. 53, no. 4, pp. 1152–1159, Jun. 2006.

[15] J. K. H. Shek, D. E. Macpherson, M. A. Mueller, and J. Xiang, "Reaction force control of a linear electrical generator for direct drive wave energy conversion," *IET Renew. Power Gener.*, vol. 1, no. 1, pp. 17–24, Mar. 2007.

[16] F. Wu, X.-P. Zhang, P. Ju, and M. J. H. Sterling, "Optimal control for AWS-based wave energy conversion system," *IEEE Trans. Power Syst.*, vol. 24, no. 4, pp. 1747–1755, Nov. 2009.

[17] L. Ran, M. A. Mueller, C. Ng, P. J. Tavner, H. Zhao, N. J. Baker, S. McDonald, and P. McKeever, "Power conversion and control for a linear direct drive permanent magnet generator for wave energy," *IET Renew. Power Gener.*, vol. 5, no. 1, pp. 1–9, Jan. 2011.

[18] R. Vermaak and M. J. Kamper, "Construction and control of an air-cored permanent magnet linear generator for direct drive wave energy converters," in *Proc. IEMDC*, Niagara Falls, ON, Canada, 2011, pp. 1076–1081.

[19] J. K. H. Shek, D. E. Macpherson, and M. A. Mueller, "Experimental verification of linear generator control for direct drive wave energy conversion," *IET Renew. Power Gener.*, vol. 4, no. 5, pp. 395–403, Sep. 2010.

[20] A. Ridge, P. Clifton, R. McMahon, and H.-P. Kelly, "Force ripple compensation in a tubular linear generator for marine renewable generation," in *Proc. IEEE IEMDC*, Niagara Falls, ON, Canada, 2011, pp. 490–495.

[21] O. Danielsson and M. Leijon, "Flux distribution in linear permanent magnet synchronous machines including longitudinal end effects," *IEEE Trans. Magn.*, vol. 43, no. 7, pp. 3197–3201, Jul. 2007.

[22] M. Rahm, C. Boström, O. Svensson, M. Grabbe, F. Bülow, and M. Leijon, "Offshore underwater substation for wave energy converter arrays," *IET Renew. Power Gener.*, vol. 4, no. 6, pp. 602–612, Nov. 2010.

[23] A. von Jouanne and P. N. Enjeti, "Design considerations for an inverter output filter to mitigate the effects of long motor leads in ASD applications," *IEEE Trans. Ind. Appl.*, vol. 33, no. 5, pp. 1138–1145, Sep./Oct. 1997.

[24] T. G. Habetler, R. Naik, and T. A. Nondahl, "Design and implementation of an inverter output LC filter used for dv/dt reduction," *IEEE Trans. Power Electron.*, vol. 17, no. 3, pp. 327–331, May 2002.

[25] H. Akagi and T. Shimizu, "Attenuation of conducted EMI emissions from an inverter-driven motor," *IEEE Trans. Power Electron.*, vol. 23, no. 1, pp. 282–290, Jan. 2008.

[26] J. Falnes, "A review of wave-energy extraction," *Marine Struct.*, vol. 20, no. 4, pp. 185–201, Oct. 2007.

[27] L. Malesani, P. Mattavelli, and S. Buso, "Robust dead-beat current control for PWM rectifiers and active filters," *IEEE Trans. Ind. Appl.*, vol. 35, no. 3, pp. 613–620, May/Jun. 1999.

[28] G. H. Bode, P. C. Loh, M. J. Newman, and D. G. Holmes, "An improved robust predictive current regulation algorithm," *IEEE Trans Ind. Appl.*, vol. 41, no. 6, pp. 1720–1733, Nov./Dec. 2005.

[29] P. Cortés, M. P. Kazmierkowski, R. M. Kennel, D. E. Quevedo, and J. Rodríguez, "Predictive control in power electronics and drives," *IEEE Trans. Ind. Electron.*, vol. 55, no. 12, pp. 4312–4324, Dec. 2008.

[30] P. P. Acarnley and J. F. Watson, "Review of position-sensorless operation of brushless permanent-magnet machines," *IEEE Trans. Ind. Electron.*, vol. 53, no. 2, pp. 352–362, Apr. 2006.

[31] M. Preindl and E. Schaltz, "Sensorless model predictive direct current control using novel second-order PLL observer," *IEEE Trans. Ind. Electron.*, vol. 58, no. 9, pp. 4087–4095, Sep. 2011.

[32] H. W. van der Broeck, H.-C. Skudelny, and G. V. Stanke, "Analysis and realization of a pulsewidth modulator based on voltage space vectors," *IEEE Trans. Ind. Appl.*, vol. 24, no. 1, pp. 142–150, Jan./Feb. 1988.

[33] S. Bolognani, S. Bolognani, L. Peretti, and M. Zigliotto, "Design and implementation of model predictive control for electrical motor drives," *IEEE Trans. Ind. Electron.*, vol. 56, no. 6, pp. 1925–1936, Jun. 2009.

[34] O. Kükrer, "Deadbeat control of a three-phase inverter with an output LC filter," *IEEE Trans. Power Electron.*, vol. 11, no. 1, pp. 16–23, Jan. 1996.

[35] A. Bouafia, J.-P. Gaubert, and F. Krim, "Predictive direct power control of three-phase pulsewidth modulation (PWM) rectifier using space-vector modulation (SVM)," *IEEE Trans. Power Electron.*, vol. 25, no. 1, pp. 228–236, Jan. 2010.

[36] P. J. Randewijk, "Multi-domain system simulation and rapid prototyping of digital control algorithms using VHDL-AMS," in *Proc. IEEE Int. Conf. Power Electron. Drive Systems*, Bangkok, Thailand, 2007, pp. 1595–1602.

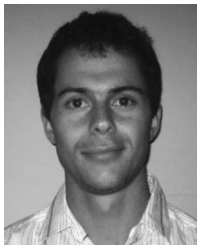

Rieghard Vermaak (M'11) received the B.Eng. degree in electrical and electronic engineering from the University of Stellenbosch, Stellenbosch, South Africa, in 2008, where he is currently working toward the Ph.D. (Eng.) degree.

He has been with the Distribution Division of South Africa's national electricity utility company, Eskom Holdings SOC Ltd., Bellville, since 2011. His current research interests are wind and ocean wave energy conversion and grid integration of renewable energy systems.

Maarten J. Kamper (M'96–SM'08) received the M.Sc. (Eng.) degree and the Ph.D. (Eng.) degree from the University of Stellenbosch, Stellenbosch, South Africa, in 1987 and 1996, respectively.

He has been with the academic staff of the Department of Electrical and Electronic Engineering, University of Stellenbosch, since 1989, where he is currently a Professor of electrical machines and drives. His research interests include computer-aided design and the control of reluctance, permanent-magnet, and induction electrical machine drives with applications in electric transportation and renewable energy.

Prof. Kamper is a South African National Research Foundation Supported Scientist and a Registered Professional Engineer in South Africa.